1e) RBC Death. After cell lysis the fraction of volume corresponding to solid unsolvable materials, wich represent approximately $V_{remain} = 6\ \mu m^3$ are left in the same spatial cell. At the end of each time step, just after merozoite propagation, these remains may fall to any of the nine nearest neighbour cells in the stratum inmediatly below, just like the RBCs do.

2a) SC Diffusion. Substrate diffusion is initially explicitly modelled with a FCTS as in Section 2.2.

$$C_{i,j,k}^{t+1} = C_{i,j,k}^{t} + \widetilde{D} \sum_{l,m,q}^{nn(i,j,k)} w_{l,m,q} C_{l,m,q}^{t} \tag{3.4}$$

l, m and q are the spatial coordinates of the 27 cells that constitute the inmediate environment of cell *(i,j,k)*. Equation 3.4 adds up the contributions of the each cell to the diffusive transport of substrate. The set of weights $w_{l,m,q}$ are:

$$w_{l,m,q} = \begin{cases} \frac{1}{2(6\sqrt{\frac{3}{2}}+3\sqrt{3}+4)} & ;\ 8\ \textit{cubic diagonals}:\ (l \neq i) \cap (m \neq j) \cap (q \neq k) \\ -1 & ;\ \textit{same spatial cell.}\ (l,m,q = i,j,k) \\ \frac{1}{2(\frac{6}{\sqrt{2}}+3+\frac{4}{\sqrt{3}})} & ;\ 12\ \textit{square diagonals, i.e.}\ (l \neq i) \cap (m \neq j) \cap (q = k) \\ \frac{1}{2(6+3\sqrt{2}+4\sqrt{\frac{2}{3}})} & ;\ 6\ \textit{square sides, i.e.}\ (l \neq i) \cap (m = j) \cap (q = k) \end{cases} \tag{3.5}$$

Substrate diffusivity is initially set to its maximum values $\widetilde{D} = 0.8$. This value is inadequate, and the submodel does not correctly account for diffusion, so it has been switched off in all the applications of INDISIM-RBC presented in this chapter. The problem regarding the model of diffusion is analyzed using other approaches in Section 3.5.2.

3.3 Analysis of experimental observations with the 3D model

3.3.1 Calibration of version *v3D*

The experimental results on the evolution of the parasitaemia for the short-term preservation (Pavanand et al., 1974) and long-term cultivation (Trager and Jensen, 1976) of *P. falciparum* in static *in vitro* cultures are used to calibrate the set of parameters employed by the model in the current version *v3D*.

The values for $\%I_0$, $\bar{t}_{INF}(t=0)$, P_{death} and P_{inf} are maintained to the ones used in version *2Dv.2* (see Sections 2.3.1 and 2.3.2). Two additional parameters are introduced

to represent specific three dimensional phenomena. The settlement of the haematocrit layer, which is modelled as the fall of individual RBCs and merozoites ($P_{fall} = 0.05$). The graphical outcome of the simulations that best fit the experimental results are presented in Figure 3.6 and extended in Ferrer et al. 2007.

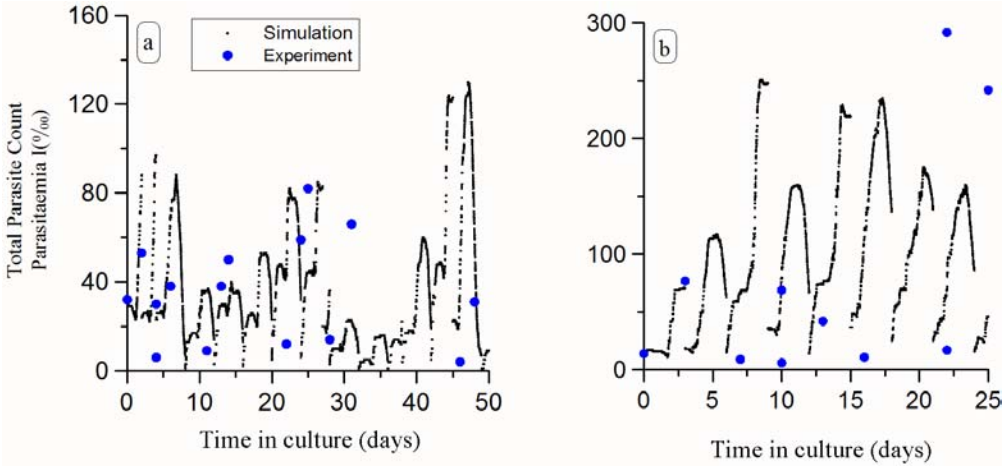

Figure 3.6: *Simulation results compared to experimental data of the overall infection course in: a) Continuous-flow static cultivation of P. falciparum; and b) static cultivation through the Candle-jar method (Jensen and Trager, 1978).*

3.3.2 Settling processes in the haematocrit layer

RBCs are slightly denser than the culturing medium. For this reason, they sink to form haematocrit layers. Once the haematocrit is formed, it can be assumed that the settling process may continue wherever there is room available in inferior levels. The subsidence of RBCs and of the material that remains after cell lysis (cell membrane and organelles that are not dissolved in the medium) through the haematocrit layer may play a role in the local limitations to the propagation of the infection. Several mechanisms modelling this settling process have been trialled, namely:

1. No fall of RBCs, merozoites and remains. Voids are left after each RBC lysis and the haematocrit layer gradually turns into a porous structure with homogeneously distributed holes containing 1 spatial cell, and bigger cavities in the regions where the infection has been spreading. These cavities caused by the successive lysis of IRBCs are empty enclosed spaces that usually contain 16 spatial cells (this is

the number of RBCs that get infected and burst during the span between two consecutive subcultivations).

These cavities do not impede nor facilitate the spreading of individual parasites, but they indirectly slow down the propagation of the infection because extracellular merozoites may spend several time steps in non occupied spatial cells.

2. RBCs, merozoites and remains fall to a lower stratum with a fixed probability P_{fall}, only if there is enough room in the spatial cell immediatly below them.

Infection growth ratios (GR) are higher when compactation methods (2 and 3) are introduced. However, the simulated GRs do not significantly vary from one mechanism to the other if the probability of falling is small enough ($P_{fall} \leq 0.05$). Simulations with the first mechanism eventually show unrealistic configurations of the haematocrit layer (for instance, a vertical profile where a stratum has nearly no RBCs while the stratums above it are full).

The sedimentation rate of real RBCs in the free culturing medium depends on many physical constraints (for instance the terminal velocity, achieved when the downward force of gravity minus buoyancy equals the upward force of drag) and physiological factors (for instance, the presence of substances promoting or inhibiting RBC adhesiveness, or the membrane potential of RBCs). The order of magnitude of the RBC sedimentation rate is around several millimeters per hour (this means that the RBC may fall down several spatial cells per time step). However, the fall of RBCs through the haematocrit layer presumably involves much slower precipitation velocities due to the interaction among cells.

The averaged cell density of the simulated haematocrit ($\overline{pf}_{sim}$) depends on the settling mechanism and on the sedimentation rate. Simulation results that fit the experimental cell density observed in the real haematocrit layers are obtained with mechanism 2 and $P_{fall} = 0.05$. Using these values, the simulated cell densities in the haematocrit layer range from $\overline{pf}_{sim} = 0.7$ to $\overline{pf}_{sim} = 0.9$.

3.3.3 Multiple invasion of RBCs

The propagation of the infection is modelled as a local invasion process that occurs when a merozoite contacts a healthy RBC with a probability described by $P_{inf}(t_{RBC})$ that varies with RBC age (t_{RBC}). Given that it is a stochastic process, the distribution of RBCs invaded by more than one parasite can be assumed to be a Poisson distribution with $\lambda = \overline{P_{inf}}$.

Following the discussion in Section 3.1.2.1, one can posit the inverse question: this is to determine the value λ that best fits the observed corrected Poisson distribution. Once this value has been set, the fraction of RBCs that are effectively susceptible to invasion can be calculated.

The distributions of multiply parasitized IRBCs that best fit with the distributions observed in real cultures (see Figure 3.7) is obtained when the model uses average invasion probabilities that range from $\overline{P_{inf}} = 0.8$ to $\overline{P_{inf}} = 1$.

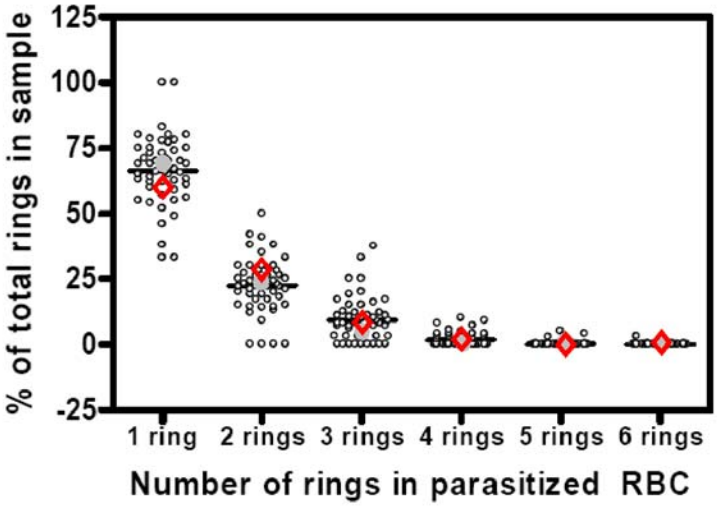

Figure 3.7: *Multiple infections expected by the model compared to experimental results observed in in vitro trials. White small circles (○): experimental counts; big solid grey circles (●): simulation outcome with the typical $P_{inf} = 0.8$; big empty diamonds (◊): simulation outcome with $P_{inf} = 1$ for all RBCs.*

Noteworthy, no significant differences are found when the values of the parameters defining P_{inf} are varied. Therefore, it can be deduced that the lack of availability of healthy RBCs is more related with local limitations on the process of spreading of merozoites, than with the values of P_{inf} .

According to the Poisson distribution that best fit experimental data, the fraction of non-infected RBCs should be $f_P(0; \lambda = 0.85) = 40\%$. Instead, the observed fraction of healthy RBCs is $f_{obs}(0) = 1 - \%I \simeq 95\%$. Therefore, the estimated fraction of RBCs that are not effectively available to the infection is around half the population of RBCs (in fact, around $\sim 55\%$).

This prediction is consistent with the rules defining the local propagation of the parasite through the haematocrit with low parasitaemia and randomly distributed IRBCs: first, as long as the parasitaemia is below 4%, the haematocrit layer is composed by unit cells that consist on one IRBC and 26 healthy RBCs; second, only 16 (on average) of these healthy RBCs can be eventually invaded by an egressed merozoite. This makes the fraction of RBCs susceptible to invasion around $\sim 60\%$.

In conclusion, the observed distribution of multiply infected parasite forms is consistent with the individual models of healthy RBC invasion and merozoite spreading.

3.4 Local limitations on the infection process

The experiments performed by EMG-GSK (see Section 3.1) reveal two system-level geometric characteristics of the haematocrit layer that affect the *in vitro* development of the parasite: depth (HLD) and separation between walls of the culturing device (L). Culture characteristics and observed results for W, B and P trials are presented in Tables 3.2 and 3.4.

The observed measurements throughout each trial show a strong time correlation, as a consequence of both the parasite infection cycle and the external manipulation of the culture system. In fact, each single trial can be regarded as the evolution of a single culture, thus characterized by the average parasitaemia throughout the whole culture trial ($\overline{\%I}$), or as a set of replicas of the evolution of the culture between two subsequent subcultivations, thus characterized by the average growth ratio (GR_{48}). The later magnitude is used to compare the trialled geometries.

The data sets from the different trials are compared one with each other using non parametric statistics, such as the Kruskal-Wallis (KW) test (see Appendix C) because GR_{48} data sets from any single trial do not come from a normal distribution. Experimental observations are also compared both to the results obtained with a system-level model, and to the outcome of INDISIM-RBC. Comparison between theoretical predictions and experimental results are carried out using parametric statistics.

3.4.1 Effect of the walls of the culturing device

Firstly, the effect of base surface (S) of the haematocrit layer on *in vitro* development of the parasite is assessed. Heuristic knowledge of the experimental group indicates that the extension of the haematocrit turns out to be important when the separation between the walls (L) of the culturing device is small enough. The data obtained from different trials (see Table 3.2) show that the development of the parasite is significantly hindered

by small separations between walls. However, the functional dependence of this hindrance on L can not be unequivocally determined: the observed average growth ratio at 48 hours from the P series can be fitted to the same degree of confidence both to a linear regression and to an inversely linear regression (see Figure 3.8).

Best fits to the experimental observations are:

the linear fit $GR_{48}^{1}(L) = 0.93 + 0.46 \cdot L$, with $r^2 = 0.86$, and

the inversely linear fit $GR_{48}^{-1}(L) = 4.67 - \frac{3.29}{L}$, with $r^2 = 0.91$.

The chi-square (χ^2) test applied to the experimental data series shows that either dependence is supported by a statistical significance of only $\sim$ 90% (there is a 10% chance of obtaining equal or better fitting results assuming that experimental data do not come from the distribution proposed by the model).

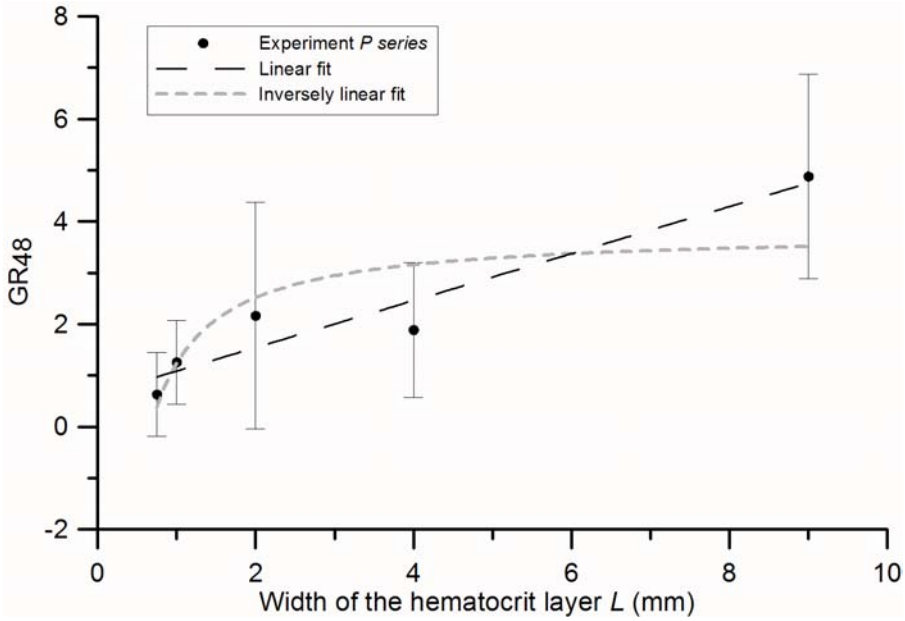

Figure 3.8: *Observed dependence of the average growth ratio at* $48\,h$ *on the distance between separators (L). Dots with error bars represent the observed data. Dashed line (–) denotes the best linear fit. Dotted grey line (· · ·) denotes the best inversely linear fit (L-model).*

System-level model of the effect of the walls (L model)

The inversely linear dependence can be explained by means of a whole-system model that considers an exclusion region in the vicinity of the walls of the culturing device where

the infection cannot progress (see Figure 3.10a). Under this assumption, the expected average growth ratio of a culture as a function of the separation between walls ($GR_{48}(L)$) is described by:

$$GR_{48}(L) = A_1 \frac{2L_{EXC}}{L} + A_2(1 - \frac{2L_{EXC}}{L}) \tag{3.6}$$

where A_2 is the growth ratio in the exclusion region (L_{EXC}), and A_1 is the bulk growth ratio ($A_1 > A_2$). The parameters that best fit this curve to the experimental data set are shown in Table 3.5. According to this fit, the exclusion region would be spread over approximately $L_{EXC} = 2.5\ mm$. Many microscopic mechanisms may be speculated as being responsible for creating this exclusion region (e. g., limitations on the spread of the metabolic waste products, hindered propagation of the parasite due to the existence of a meniscus) but it is not possible to discriminate among them with the current information. The observed exclusion region is consistent with the expected exclusion region induced by the capillary length (L_C) of the culture medium, but not by capillarity of the haematocrit layer (see Section 3.1.2.3).

3.4.2 Effect of the haematocrit layer depth

The KW test showed that data obtained from W and B series come from the same distribution function with significance greater than 99.9%. For this reason, all the measurements have been grouped in a single data sample. Average values are given for the data corresponding to similar geometric conditions, for each of the subgroups: {W3+B1}, {W4+B2+B3} and {W5+B4+B5}.

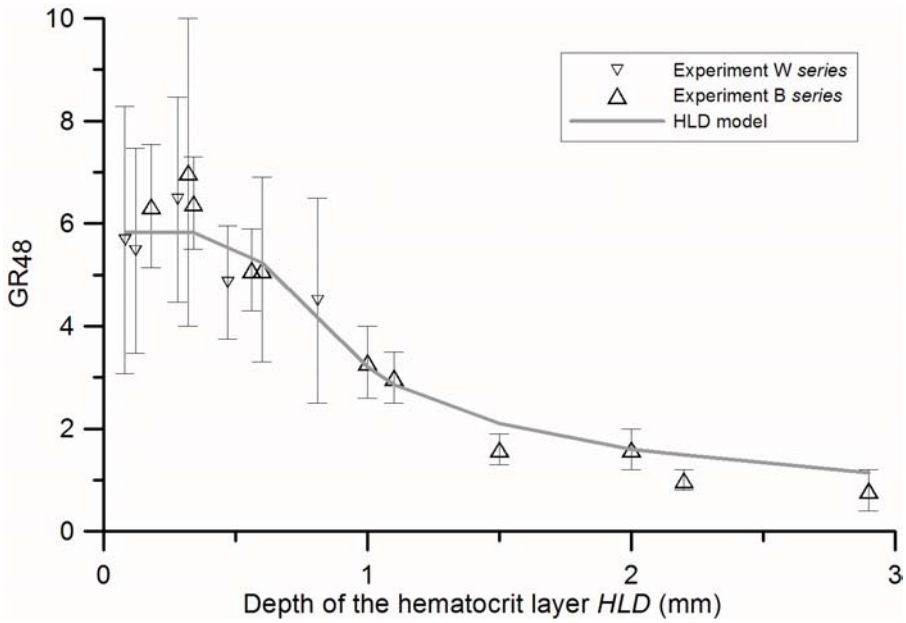

Figure 3.9: *Dependence of the parasitaemia on the haematocrit layer depth (HLD). Triangles with error bars represent the observed data of W (▽) and B (△) series. The solid line denotes the best fit for the system-level model* HLD.

Experimental data show asymptotic inversely linear behaviour for large values of HLD (Figure 3.9). Optimum parasite development occurs in cultures with HLD between $0.18\ mm$ and $0.34\ mm$.

System-level model of the effect of haematocrit layer depth (*HLD* model)

A simple system-level model that reproduces the observed behaviour consists in splitting the haematocrit layer into discrete regions that have different behaviours. The inversely linear decay for deep cultures is reproduced when the haematocrit layer is split into two horizontal regions: $HLD = h_1 + h_2$. The first region has a fixed depth $h_1 = h$ and shows a high fixed infection multiplication ratio B_1, while the infection spreads at a lower rate ($B_2 < B_1$) in the remaining part of the haematocrit layer ($h_2 = HLD - h$, see Figure 3.10b). Let B_1 and B_2 be the multiplication ratio per infection cycle in each of the above mentioned subregions, and HLD the total depth of the haematocrit layer. The average infection growth ratio at 48 h, $GR_{48}(HLD)$ is then given by:

$$GR_{48}(HLD) = \begin{cases} B_2 + (B_1 - B_2) \cdot \frac{h}{HLD} & if\ HLD > h \\ B_2 & if\ HLD < h \end{cases} \tag{3.7}$$

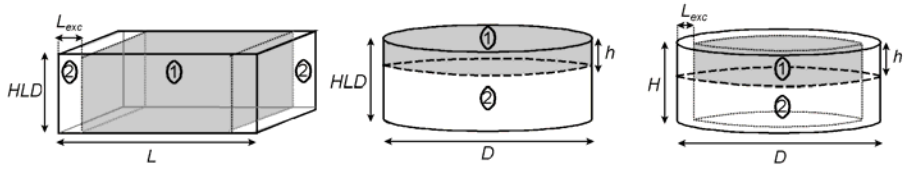

Figure 3.10: *Depiction of the whole system model of the haematocrit layer. a) Schema of the culture system according to the model used to tackle P trials. HLD indicates haematocrit layer depth, L stands for the separation between walls of the culturing device and L_{exc} represents the extent of the exclusion region, where the spread of the infection is hindered. The shaded subregion (1) indicates the fraction of the haematocrit layer where the rate of infection spreading is high. b) Schema of the culture system according to the model used to tackle B and W trials. HLD indicates haematocrit layer depth, D stands for the diameter of the haematocrit layer and h represents the extent of the exclusion region, where the spread of the infection is hindered. The shaded subregion (1) indicates the fraction of the haematocrit layer where the rate of infection spreading is high. c) Schema of the model to tackle all the geometric effects simultaneously. The propagation of the infection is hindered both by the walls of the culturing device and by diffusive limitations. The shaded subregion (1) indicates the fraction of the haematocrit layer where the rate of infection spread is high.*

The parameters that define the curve that best fits with the experimental data set are shown in Table 3.5. The parameters have been estimated using a numerical approximation, and their likelihood given the observations has been checked using both the Kolmogorov-Smirnoff (KS) test and the chi-squared test (χ^2). The former statistic has been taken as the reference for the statistical significance of likelihood, because it implies fewer restrictions on both data sets and provides a smaller value for the degree of confidence of the results.

3.4.3 Whole-system model that accounts for HLD and L together (WS model)

The models presented in sections 3.4.1 and 3.4.2 can be merged into a system-level representation of the whole culture (Figure 3.10c). The evolution of the culture as a

function of the geometric variables L and HLD is shown in:

$$GR_{4S}(L;HLD) = \begin{cases} K_2 + (K_1 - K_2) \cdot \frac{h}{HLD} \cdot (1 - \frac{2L_{EXC}}{L}) & if\ HLD > h \\ K_1 \frac{2L_{EXC}}{L} + K_2(1 - \frac{2L_{EXC}}{L}) & if\ HLD < h \end{cases} \quad (3.8)$$

The values for L_{EXC} and h have been adopted from the best fit values found in sections 3.4.1 and 3.4.2. The two other parameters (K_1 and K_2) refer to the growth ratios in the subregions with high and low parasite propagation, respectively, and are calculated from the best fit to experimental data. The obtained values are presented in Table 3.5. A graphical comparison between the theoretical predictions and the experimental behaviour is shown in Figure 3.11. The KS test applied to expected and observed data sets gives a confidence between 90% and 95% for the proposed model.

System-level model	Characteristic parameters			p-value
L-model	A_1	A_2	L_{EXC} (mm)	
	4.1	0.6	2.45	0.03
HLD-model	B_1	B_2	h (mm)	
	5.8	0.4	0.48	< 0.001
WS-model	K_1	K_2	h, L_{EXC}	
	5.4	0.4	set	0.0012

Table 3.5: *Characteristic parameters of the continuous models defined at a system level of description that best reproduces the experimental observations.* L-model *considers the effect of the distance between the walls of the culturing device, and* L_{EXC} *is the region near the walls of the culturing device where the propagation of the parasite is hindered;* HLD-model *considers the effect of the depth of the hematocrit layer, with* h *the horizontal subregion where the propagation of the parasite is not hindered;* WS-model *merges both models and aims to reproduce the culture behaviour for any geometric layout,* L_{EXC} *and* h *have maintained their values from the best fits obtained with the* L- *and the* HLD- *models. The values for the parameters* K_1 *and* K_2 *have been set through the optimization of the likelihood of the model outcome to experimental data. Significance of the obtained results (p-value) has been assessed using the Kolmogorov-Smirnoff (*KS*) test; p-values represent the probability of obtaining better results assuming the null hypothesis.*

This merging allows checking of the consistency of the models proposed above both with each other and with the experimental observations. It enables the specification of the most appropriate geometric conditions for the static in vitro cultures of *P. falciparum* infected erythrocytes.

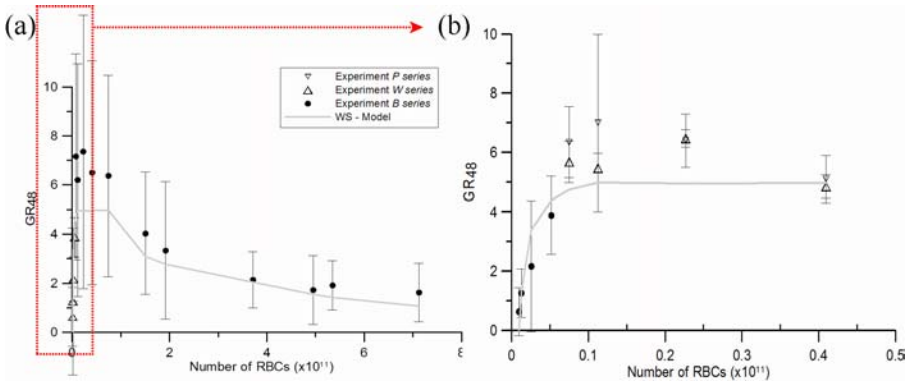

Figure 3.11: *Dependence of the parasite growth ratio (GR_{48}) both on the haematocrit layer depth (HLD) and width (L), represented together as the number of cultured RBCs. Solid dots (•) with error bars represent observed data from P trials. Empty triangles with error bars represent the averaged observed values from W (△) and B (▽) trials. The solid line (-) represents the best fit values provided by the WS model. a) Experimental data sets from W and B trials on the whole; b) detailed view of trials with small culturing volumes.*

3.4.4 Outcome of INDISIM-RBC

The experimental results have been compared with the corresponding outcome of the simulations carried out with a version of INDISIM-RBC.*v3D* that accounts for whole-system model. The WS assumptions have been introduced as *ad hoc* constraints on the rules governing the individuals (parasites and RBCs) at a cellular and local level. The simulation space is split into two horizontal sub-regions (layers 1 and 2, respectively; see Figure 3.4.3b) with different probabilities of infection ($P_{inf}(1)$ and $P_{inf}(2)$, respectively). The simulations also allow assessing the effect of the walls on real cultures. This is implemented through placing a vertical wall on one of the side boundaries of the simulation space, this is changing one of the periodic boundary conditions for a pair of closed and open boundary walls facing each other.

INDISIM-RBC is used to tackle solely the geometric constraints on parasite proliferation at a cellular level, so just a few parameters from the general model are modified: P_{max} is set to $P_{inf}(1)$ and $P_{inf}(2)$ at each of the subregions. The probability of infection for mature RBCs ($P_{min} = 0$), the rate of local spreading of merozoites ($P_{fall} = 0.05$) and all the remaining parameters have been held to the values fixed by the simulation results of the *candle-jar* method (see Section 3.3.1). The estimated values for $P_{inf}(1)$ and $P_{inf}(2)$ are those that provide the simulation outcomes that best fit with the macroscopic

observations on the average growth rate at 48 hours (GR_{48}), and they are presented in Table 3.6.

Characteristic parameters of the IBM	$p_{inf}(1)$	$p_{inf}(2)$	p_{fall}	Significance
Best fit values	0.51	0.01	0.05	0.014

Table 3.6: *Characteristic parameters of the Individual-based model that best reproduce the experimental observations. The values for the parameters representing the infection probability in the upper (1) and lower (2) regions of the hematocrit layer ($p_{inf}(1)$, $p_{inf}(2)$) as well as the sedimentation rate (P_{fall}) have been set through the optimization of the likelihood of the model outcome to experimental data. Significance of the obtained results has been assessed using the Kolmogorov-Smirnoff* (KS) *test; the presented values show the probability of obtaining better results with the null hypothesis.*

A graphical comparison between the outcome of the IbM and the whole-system models is shown in Figure 3.12. The estimation of the optimal values has been carried out through systematic, yet not exhaustive exploration of the space of parameters; better fits could be found by the recursive refinement of the optimization protocol. Such an improvement of the values at a cellular level has not been carried out because parameters such as P_{inf} stand for very specific characteristics of the parasite strain, blood sample and culturing conditions. Thus the accurate estimation of the best-fit values does not provide general insight concerning the culture system. The likelihood of the simulation results, given the experimental observations, has been checked using both the Kolmogorov-Smirnoff (KS) test and the chi-squared test (χ^2). Again, the former statistic has been taken as the reference for the statistical significance of the likelihood, because it implies fewer restrictions on both data sets and it provides a smaller value for the degree of confidence of the results.

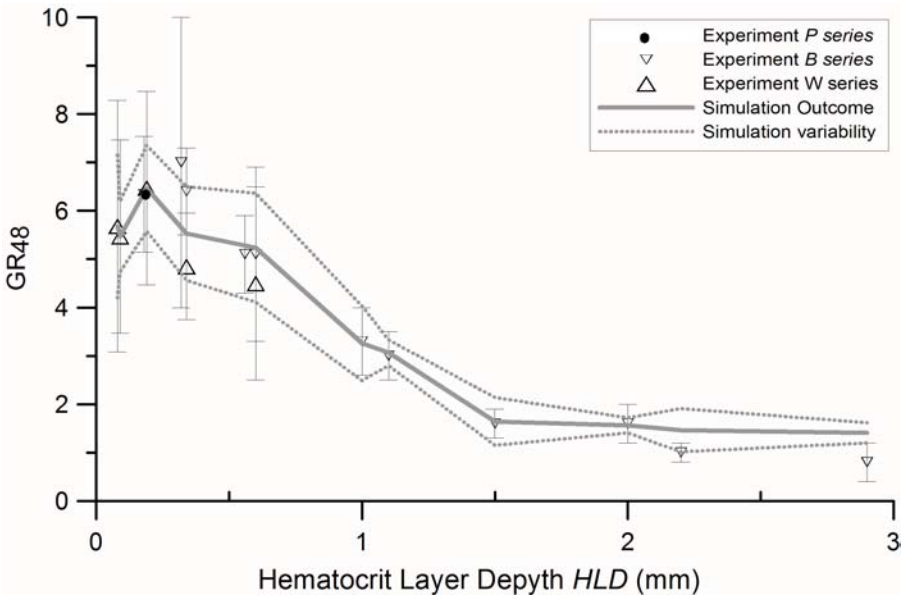

Figure 3.12: *Dependence of the growth ratio of the simulations on the haematocrit layer depth (HLD). Symbols with errorbars represent the observed data, (•: P-series, △:W-series and ▽: B-series). Grey solid line denotes the best fit for the IINDISIM-RBC simulation outcomes. Dashed lines represent the deviation in the outcome observed for 4 simulation runs of each of the observed points.*

3.4.5 Discussion

The systematic study of different macroscopic culturing conditions has allowed for the building of a quite simple whole-system model which is compatible with the experimental observations and which may account for some and yet poorly understood phenomena.

Some conclusions may be drawn from the experimental results, assuming the whole-system model:

1. Cell-cell interactions such as erythrocyte aggregation and rosette formation around parasitized cells can be accounted for as average intercellular binding energy that determines the macroscopic shape of the haematocrit layer in the *in vitro* cultivation of *P. falciparum*-infected erythrocytes. Under custom culturing conditions, the haematocrit layer can be considered as a flat film, but such depiction is not valid when the haematocrit volume decreases. At small volumes of haematocrit the intracellular binding energy (which can be tackled as a surface tension on the

haematocrit boundaries) is comparable to gravitational energy, so the haematocrit must be regarded as a sessile drop at the macroscopic scale. Different shapes of the haematocrit are observed depending on the material of the culturing device.

2. According to the L-model, the spread of the infection is hampered by short distances between walls (L), and cultures have are expected to be strongly hindered when $L < L_{EXC} \sim 2.5\ mm$. By extrapolating Equation 3.6, it is deduced that the effect of the exclusion region can be overlooked in the WS-model when $L > 2\ cm$ with more than 95% confidence.

3. The geometric conditions of the culture systems at a macroscopic level of description play an important role in parasite development. According to the HLD-model, the spread of the infection is hampered for thick haematocrit layers. In particular the hindrance appears when the depth of the haematocrit layer exceeds a maximum threshold value $HLD > h \sim 0.478\ mm$.

4. A bottom-up approach can be used to check the validity and consistency of the system-level models. The simulation outcomes are consistent with observations when the haematocrit layer is split into two subregions. Such an IbM also enables specific study and treatment of the relevant processes occurring at the scale of the parasite. As a result, some additional conclusions may be drawn from analysis of the IbM:

   (a) The maximum threshold for the growth ratio at the zone of high parasite proliferation is geometrically fixed: the multiplication of the number parasite is not enough to ensure an appropriate GR_{48}, but a minimum spreading of the merozoites is also required. This is shown by the model because increasing the maximum probability of individual infection (P_{inf}) above a certain threshold value does not entail an increase in the infection growth ratio. In contrast, greater diffusion rate for the extracellular parasite through the haematocrit layer (P_{fall}), or the slight rift of RBCs (P_{fall}) does affect the global growth ratio.

   (b) The macroscopic subregions of different parasite proliferations (layers 1 and 2 in Figure 3.10b) are externally imposed on INDISIM-RBC as *ad hoc* modifications on the rules governing the parasite proliferation at a local level. The reduction of subregion 1 in Figure 3.10c can be recreated with the IbM as a consequence of the perturbations caused by introducing a closed boundary into the simulation. The quantitative reproduction of the observed behaviours

has not been achieved because simulations representing the whole haematocrit layer are unfeasible due to excessive computation demands.

(c) The observed reduction in the average GR_{48} for very thin haematocrit layers (unfeasibility of the harvest when $HLD < 0.04\ mm$, and noticeable hindrance on cultures with $HLD < 0.1\ mm$) is reproduced with INDISIM-RBC even though it has not been introduced as an *ad hoc* external input on the rules governing the model. This is an example of an emergent behaviour that arises from the local interactions among individuals. It is caused by the effect of the existence of a closed boundary of the system on the propagation of the parasite.

According to the obtained results as a whole, most appropriate dimensions of tested HLDs range from $0.18\ mm$ up to $0.34\ mm$ and most convenient distances must exceed $L > 2\ cm$.

To sum up, the systematic study of a wide range of geometric configurations for the haematocrit layer allows for predictive capacity formalized in a system-level phenomenological model. The resulting whole system model is consistent with INDISIM-RBC as soon as the haematocrit layer is split into two subregions with different infection proliferation rates.

The bottom-up approach can not provide justification for the *ad hoc* phenomenological laws. In particular, the mechanism responsible for the emergence of two phases in the haematocrit layer is not included (but just assumed) in INDISIM-RBC. Heuristic arguments support that limitations are due to the local scarcity of substrate in deep regions of the haematocrit layer, as a consequence of a limited diffusion.

3.5 Local substrate limitations in the hematocrit layer

The differences observed between different geometries in the static *in vitro* cultures of *P. falciparum* infected erythrocytes have been reproduced in Section 3.4.4 by defining a model that splits the haematocrit layer (HL) into two subregions: one with plentiful proliferation of the parasite and the other where the infection is hindered.

This section analyses how diffusion of substances through the haematocrit layer can affect the viability of healthy and infected cells RBCs and lead to the formation of these two regions. *Grosso modo:* RBCs need a continuous supply of substrate and a clean surrounding in order to maintain their viability (IRBCs are even more demanding and dump more metabolic waste). During the course of the cultivation, the activity of cells

leads to the local exhaustion of the medium, which appears more markedly around the IRBCs (see Section 2.3.5). The degradation of the environment can harm or even kill the RBCs, thus hindering or even stopping the proliferation of the infection.

3.5.1 Diffusion limitations in the haematocrit layer

Diffusion limitation in static cultures arises from the joint effect of the individual uptake and the limited diffusivity through the haematocrit layer. Diffusion in the haematocrit layer can be correctly described with the reaction-diffusion equation (Eq. 3.9), which relates the temporal variation of the concentration ($C(\overrightarrow{x},t)$) at a given point ($\overrightarrow{x}$) characterized by the fraction of diffusing medium ($\epsilon_w = 1 - pf$, the fraction of volume not occupied by the cells), with the mechanisms that cause it:

i) the diffusion term, which is proportional to the second derivate of the concentration ($\triangle C = \sum_{i=1}^{N} \frac{\partial^2 C(\overrightarrow{x},t)}{\partial x_i^2}$) and to the effective diffusivity (D_e), and

ii) the reaction term, which accounts for local consumption of substrate or average uptake rate ($U(C)$).

$$\epsilon_w \frac{\partial C(\overrightarrow{x},t)}{\partial t} = D_e \cdot \triangle C(\overrightarrow{x},t) - U(C(\overrightarrow{x},t)) \tag{3.9}$$

The values for the effective diffusivities in the haematocrit layer are taken from literature and presented in Table 3.7.

	Free Culture Medium	haematocrit Layer
Glucose	$D_0 = 9.3 \cdot 10^{-6}\ cm^2/s$	$D_{eff} = 0.24 \cdot D_0 = 2.2 \cdot 10^{-6}\ cm^2/s$
Lactate	$D_0 = 1.5 \cdot 10^{-5}\ cm^2/s$	$D_{eff} = 0.19 \cdot D_0 = 2.9 \cdot 10^{-6}\ cm^2/s$

Table 3.7: *Effective diffusivities of glucose and lactate through the Free Culture Medium (FCM), and through the haematocrit layer (HL). Diffusivities in the FCM are set to their respective values in water (Jou, 1985). The value of the effective diffusivities in the HL is averaged from measures in biofilms (Stewart, 1998).*

The haematocrit layer is modeled as a flat infinite film with an averaged homogeneous distribution of IRBCs. Only the limitations on the RBC viability resulting from the local scarcity of glucose are taken into account. In consequence, the diffusion problem is reduced to a problem in 1D: assessing the variations of the concentration of glucose in the direction normal to the haematocrit surface (z), $C(z,t) = C_{gluc}(\overrightarrow{x} = (\forall, \forall, z); t)$.

Two models of the averaged uptake have been considered i) a fixed uptake rate (zero-order kinetics), and ii) a linear dependence of the uptake with the concentration of glucose

until reaching a maximum value (first-order kinetics).

Diffusion limitation for a 1D model with zero-order kinetics

Zero-order kinetics states that the uptake in Equation 3.9 is a constant value: $U(C(\overrightarrow{x},t)) = \overline{U}_{HL}$. The averaged uptake of a culture with $\%I \sim 0.5\%$ is $\overline{U}_{HL} = 4.7{\cdot}10^{-7} mol{\cdot}l_{RBCs}^{-1}{\cdot}s^{-1}$ (Rapoport et al., 1976). The effective volume available for diffusion is the fraction of volume not occupied by RBCs ($\epsilon_w = 1 - \overline{pf} = 0.15$). The relevant characteristics of the culture system are HLD and the bulk concentration of substrate in the culturing medium ($C_0 = 2.67\ mM/l$). Equation 3.9 can be rewritten in the following adimensional form:

$$\frac{\partial \widetilde{C}(\zeta,\tau)}{\partial \tau} = \frac{\partial^2 \widetilde{C}(\zeta,\tau)}{\partial \zeta^2} - \psi^2 \frac{\overline{U}_{HL}}{C_0} \tag{3.10}$$

where $\tau = \frac{t \cdot D_{eff}}{(1-pf)\cdot HLD^2}$ and $\zeta = \frac{z}{HLD}$ are adimensional time and length, respectively; $\widetilde{C}(\zeta,\tau) = \frac{C(\zeta,\tau)}{C_0}$ is the instantaneous substrate concentration profile, normalized to the concentration at the free culturing medium; and $\psi^2 = \frac{(1-pf)\cdot HLD^2}{D_{eff}}$ is a scaling factor.

The contour conditions for Equation 3.10 are:

i) $C(1) = C_0$, meaning that the concentration in the top of the HL is equal to the bulk concentration. This is actually a superestimation of its real value, because a diffusion boundary layer (DBL) should be considered above the top of the HL.

ii) $C'(0) = 0$, meaning that there is no flux in the bottom of the HL because there is a wall at the bottom of the culturing system.

A maximum threshold to the concentration profile is obtained by considering diffusion alone. If the uptake is neglected ($\overline{U}_{HL} = 0$), Equation 3.10 with the contour conditions (i) and (ii) has an analytical solution, which is easily obtained with the Laplace transform ($\widetilde{c}(\zeta,s) = \mathcal{L}\left[\widetilde{C}(\zeta,t)\right]$). The solution of this algebraic equation in the frequency domain (s) is (Stewart, 1996):

$$\widetilde{c}(\zeta,s) = \frac{cosh(\sqrt{\frac{s}{D_{eff}}}\cdot\zeta)}{s\cdot cosh(\sqrt{\frac{s}{D_{eff}}})} \tag{3.11}$$

The corresponding solution in the temporal domain is given by an infinite series of trigonometric terms, with every term multiplied by the factor $e^{-\frac{t}{\psi^2}}$ that tends to zero when $t \to \infty$ (Crank, 1990). Such a solution corresponds to a substrate profile that

graphically resembles a complementary error function with a variance that increases with t (see Figure 3.13). In the limit $t \to \infty$, the concentration profile is a homogeneous distribution $\widetilde{C}(\zeta, \infty) = 1, \forall\zeta$.

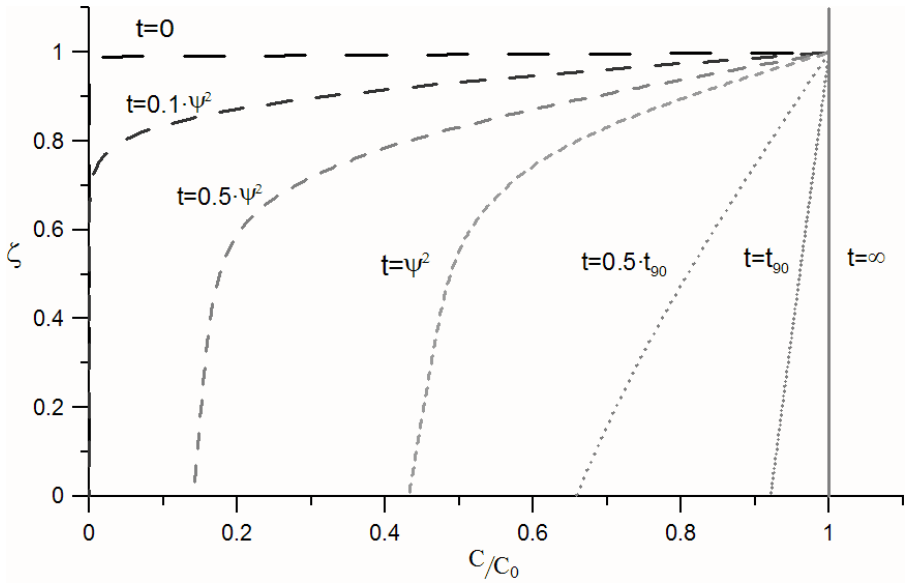

Figure 3.13: *Temporal succession of the normalized vertical profiles of glucose concentration ($C(\zeta, t)$) through the levels of the haematocrit layer (ζ). Initially ($t = 0$), $C(\zeta, 0) = C_0$ in the bulk culture medium ($\zeta > 1$) and $C(\zeta, 0) = 0$ in the haematocrit layer ($\zeta < 1$). The bulk concentration is maintained $C(1, t) = C_0$, and glucose accumulates at $\zeta = 0$, $\frac{\partial C(0,t)}{\partial t} = 0$. Diffusion makes the substrate penetrate the layer until reaching a uniform concentration $C(\zeta, \infty) = C_0$; ψ^2: characteristic temporal scale of the diffusion process; $t_{90} = 7\psi^2$, when $C(0, t_{90}) \simeq 0.9\Delta C_0$.*

The characteristic temporal scale of the diffusion process is defined by the scaling factorψ^2. A typical measurement of this characteristic scale is $t_{90} = 7\psi^2$, which stands for the time when the concentration of a substances at the bottom of the cultured layer reaches $\sim 90\%$ of its value at the bulk medium, as a consequence of diffusion alone, $\widetilde{C}(0, t_{90}) = 0.9$ (Stewart, 2003). In the limit $t \to \infty$, the concentration profile reaches a steady state that does not vary with time. The substrate concentration profile of the steady state ($C_{st}(\zeta)$) is reached when $t > t_{90}$, and is given by:

$$C_{st}(\zeta) = C_0 - \frac{\overline{U}_{HL} \cdot HLD^2}{2 \cdot D_{eff}} \cdot (1 - \zeta^2) \tag{3.12}$$

The static cultures studied in this work (*P*-, *W*- and B-series) reach the steady state before the subcultivations take place (see Table 3.8). This means that the steady solution $C_{st}(\zeta)$ can be considered a good approximation to the concentration profiles in the haematocrit layer.

The characteristic spatial scale of the zero-order reaction-diffusion model (Eq. 3.10) in the steady state ($t > t_{90}$) is given by the depletion depth (Stewart, 2003):

$$d_0 = \sqrt{\frac{2 \cdot D_{eff} \cdot C}{\overline{U}_{HL}}} \tag{3.13}$$

Once the steady state has been reached, d_0 represents the level (position in the z direction) below which the concentration of substrate is zero. In the *P*-, *W*- and *B*-series: $C = C_0 = 2.67\Delta 10^{-3} mols/l$, $D_e = 2.2\Delta 10^{-6} cm^2/s$. According to the zero-order approximation, $\overline{U}_{HL} = 4.7 \cdot 10^{-7} mol \cdot l^{-1}_{RBCs} \cdot s^{-1}$. As a result: $d_0 = 1.6\ mm$.

Other characteristic scales may be useful for the current analysis: d_{RBC} and d_{IRBC}. They represent the levels of the *HL* that have enough can hold RBCs and IRBCs, respectively. These levels are placed above the depletion depth and fulfill: $d_{RBC} > d_{IRBC}$.

These characteristic levels define three different subregions in the haematocrit layer:

1) $z > HLD - d_{IRBC}$, where both RBCs and IRBCs have enough substrate to fulfill their metabolic needs in the stationary state.

2) $HLD - d_{RBC} > z > HLD - d_{IRBC}$, where RBCs have enough substrate but IRBCs don't, in the steady state.

3) $HLD - d_{RBC} > z$, where there is not enough available nutrient to fulfill the RBCs metabolic needs in the stationary state.

The growth ratio measured for a culture system is the average of the contributions of subregions (1), (2) and (3). With regards to the overall observed performance of the culture system, these three subregions define three expected behaviors.

i) $GR(HLD)$ is maintained to a maximum value, for those cultures where both healthy and infected RBCs are viable. $GR(HLD) = GR_{max}$ as long as $HLD < d_{RBC}$.

ii) $GR(HLD)$ decreases with HLD in those cultures that allow two different subregions for the viability of the IRBCs, as long as the ratio of the volumes of both regions ($\frac{V(1)}{V(2)}$) is varied. $GR(HLD) = GR_{max} \cdot \frac{d_{IRBC}}{HLD}$ while $d_{RBC} > HLD > d_{IRBC}$.

iii) $GR(HLD)$ is maintained to a minimum value when the thickness of the culture exceeds the region of RBC viability. $GR(HLD) = GR_{min} = GR_{max} \cdot \frac{d_{IRBC}}{d_{RBC}}$ as long as $HLD > d_{RBC}$

The values $d_{RBC}$and d_{IRBC} can not be estimated with the current approximation, because the model does not consider different uptake regimes for RBCs and IRBCs, but an averaged overall uptake rate.

Diffusion limitations with first-order kinetics

First-order kinetics states that the uptake in Equation 3.9 is described with the following function:

$$U(C(z,t)) = \begin{cases} U_{max} & ; \; if \; C < C_{max} \\ \frac{K_{eff}}{pf} \cdot C(z,t) & ; \; if \; C < C_{max} \end{cases} \tag{3.14}$$

The values for the maximum uptake rate are $U_{max}(RBCs) = 4.7 \cdot 10^{-7} mol \cdot l_{RBCs}^{-1} \cdot s^{-1}$ and $U_{max}(IRBCs) = 4.7 \cdot 10^{-5} mol \cdot l_{RBCs}^{-1} \cdot s^{-1}$, respectively (see Equation 2.3).

Two measurements taken from literature are used to define the parameters in this model: the kinetic constant for the glucose slow uptake phase $K_{eff} = 0.016 \; min^{-1}$and the saturation concentration, at which RBCs uptake at their maximum rate $C_{max} = 40 \; mM$ (Leitch and Carruthers, 2007).

Equation 3.14 allows defining the threshold glucose concentrations below which the uptake requisites of healthy RBCs and IRBCs are not fulfilled. These concentrations (C_v) determine the viability of healthy and infected cells. Their values are $C_V(RBC) = 2.4 \cdot 10^{-5} mols/l$ and $C_V(IRBC) = 2.4 \cdot 10^{-3} mols/l$, respectively.

The values $C_V(RBC)$ and $C_V(IRBC)$ can be introduced in Equation 3.13, assuming $C = C_0 - C_v$, to obtain a coarse estimation of the threshold depths for cell viability: $d_{RBC} = 1.6 \; mm$ and $d_{IRBC} = 0.5 \; mm$.

The assumption of constant depletion depths (independent from the HLD of the culture) constitutes the so called *K*-model. The decrease in the culture performance ($GR_{48}(HLD)$) with HLD predicted by *K*-model is depicted in Figure 3.15 and compared with the predictions of other diffusion models described below.

Optimal HL depth estimated with the Thiele modulus

Splitting the *HL* into three subregions with fixed thicknesses is indeed a coarse approximation. In real systems, the uptake rate (reaction term in Equation 3.9) explicitly

depends on the concentration profile ($C(z,t)$), which even in the steady state is affected by HLD (see Equation 3.12). Consequently, the values d_{RBC} and d_{IRBC} must be affected by *HLD* and can not be taken for constants. An alternative approach is required.

An adimensional number usually employed in the study of diffusion-reaction processes is the Thiele modulus (ϕ), defined as the ratio between the reaction rate and the diffusion rate. The Thiele modulus allows for the distinction between two regimes in the reaction-diffusion models. If ϕ is small, diffusion is fast compared to reaction, but when is large ($\phi \gg 1$), diffusion is slow (Stewart, 1996).

Assuming zero-order kinetics in a flat thin layer, the Thiele modulus ϕ_0 and the normalized substrate concentration profile achieved once the reaction diffusion reaches the steady state $\widetilde{C^0_{st}}(\zeta)$ are defined as:

$$\phi_0 = \sqrt{\frac{pf \cdot \overline{U_{HL}} \cdot HLD^2}{D_{eff} \cdot C_0}} \quad ; \quad \widetilde{C^0_{st}}(\zeta) = \begin{cases} 0 & ; if\ 0 \leq \zeta \leq (1 - \frac{1}{\phi_0}) \\ (1 - \phi_0 - \phi_0\zeta)^2 & ; if\ (1 - \frac{1}{\phi_0}) \leq \zeta \leq 1 \end{cases} \tag{3.15}$$

For the first-order kinetics, ϕ_1 and the corresponding $\widetilde{C^1_{st}}(\zeta)$ are defined as:

$$\phi_1 = \sqrt{\frac{(1-pf) \cdot K_{eff} \cdot HLD^2}{D_{eff}}} \quad ; \quad \widetilde{C^1_{st}}(\zeta) = \frac{cosh(\phi_1 \cdot \zeta)}{cosh(\phi_1)} \tag{3.16}$$

The calculated values of ϕ_0 and ϕ_1 for the different HLD are listed in Table 3.8. The vertical profiles obtained for different values of the Thiele modulus are depicted in Figure 3.14.

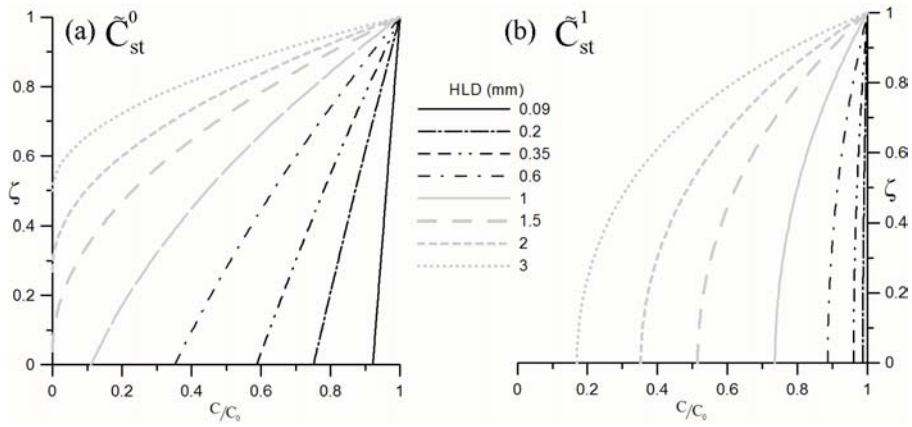

Figure 3.14: *Expected normalized glucose concentration profiles at the steady state* $\widetilde{C}_{st}(\zeta) = \frac{C}{C_0}$ *for different haematocrit layer depths (HLD). a) Predictions of the zero-order kinetics model (see Equation 3.15); b) Predictions of the first-order kinetics model (see Equation 3.16)*

The depletion depths d_{RBC} and d_{IRBC} can be calculated using these profiles and the estimated threshold concentrations of cell viability (see Equations **??** and **??**). They are listed in Table 3.8. As expected, the values for d_0, d_{RBC} and d_{IRBC} decrease with HLD: more cells entail a more severe exhaustion of the medium.

The concentration gradients obtained assuming zero-order kinetics (0-model) are greater than those obtained assuming first-order kinetics (1-model) because the former fixes a constant consumption of nutrient within the viability region, while the uptake continually decreases with nutrient concentration under first-order kinetics.

No measurements of the concentration profiles have been carried out for the experimental culture systems, so it is not possible to determine which model provides a better approximation to reality. However, the goodness of these models can be indirectly determined through comparing the expected decrease in the culture performance ($GR_{48}(HLD)$) with HLD predicted by each model.

Expected infection growth rates

The threshold depths for RBC and IRBC viability (d_{RBC} and d_{IRBC}) obtained with the K-model, 0-model and 1-model can be used to determine the values of the key pa-

rameter h of the HLD-model (and the WS-model) (see Equations 3.7 and 3.8):

$$h = \begin{cases} HLD & ; if\ HLD < d_{IRBC} \\ d_{IRBC} & ; if\ d_{IRBC} < HLD < d_{RBC} \\ HLD \cdot \frac{d_{IRBC}}{d_{RBC}} & ; if\ d_{RBC} < HLD \end{cases} \tag{3.17}$$

The expected growth ratios $GR_{48}(HLD)$ obtained when the value h is defined using Equation 3.17 are depicted in Figure 3.15, together with the experimental values and the best-fit model.

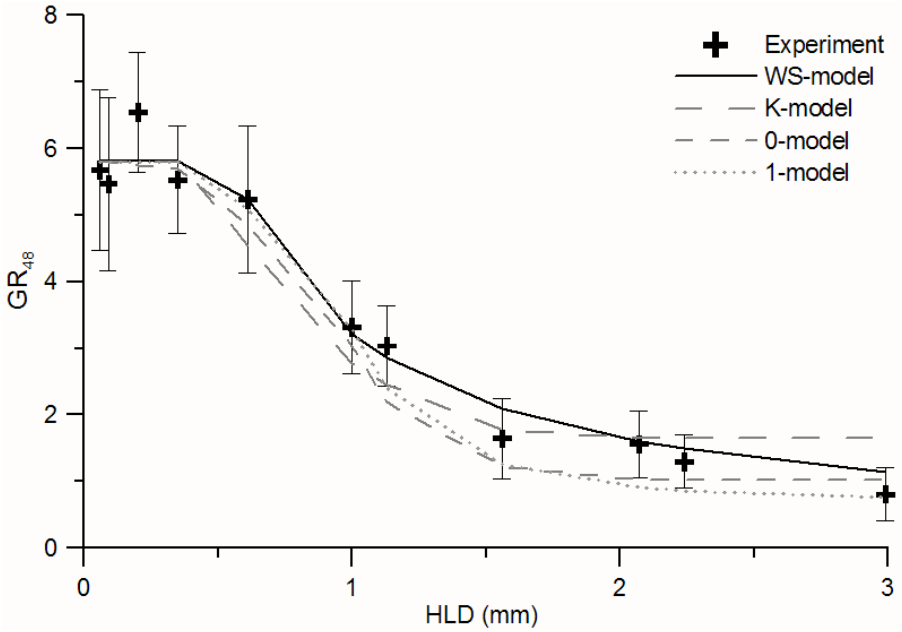

Figure 3.15: *Average infection growth ratio (GR_{48}) as a function of the haematocrit layer depth (HLD). Crosses (+): experimental results; black solid line: best-fit HLD-model (see Section 3.4); long-dashed line: results obtained with the K-model; short-dashed line: results obtained with the 0-model, dotted line: results obtained with the 1-model.*

The obtained results show that models considering just one dimensional diffusion limitations qualitatively follow the trends observed in the experimental haematocrit layers, but still fail to reproduce the behaviour of real systems. Apart from the decay for very thin HLs ($HLD < 0.1\ mm$) (which can be explained as an emergent behaviour of merozoite propagation, see Section 3.4), there are two main differences between the predicted and

observed $GR_{48}(HLD)$: firstly, the decrease with HLD is greater in the diffusion models than in real systems. Secondly, for thick HLs ($HLD > d_{RBC}$), the slope of GR_{48} is flat, while in the experimental systems and best-fit WS-model $\frac{dGR_{48}}{dHLD} < 0$ in all the explored domain.

The first difference can be explained as the result of considering a constant uptake for a RBC population that is not affected by nutrient availability. The models here presented can not take into account mortality due to the scarcity of substrate. In real systems the average uptake will be drastically reduced below the depletion boundary. As a consequence, the thickness of the layer with no substrate limitations (h) will be increased.

The second difference, the asymptotic $GR_{48}(HLD)$ is a consequence of the definition of h for thick HLs (see Equation 3.17). It is observed in the K-model and 0-model alone, while the 1-model does not show this behaviour because all the trialled HL fulfill $HLD < d_{RBC}$. Nevertheless, there is a slight difference on how the K-model and the 0-model define the extension of the subregion with high infection propagation: in the K-model $d_{RBC}$and d_{IRBC} are fixed values while in the 0-model both distances vary with HLD ($d = d(HLD)$) and what remains almost fixed is the ratio $\frac{d_{IRBC}}{d_{RBC}}$.

Another key difference between the WS-model and the diffusion models presented in the current section lies in the fact that the former defines two subregions in the HL with different infection propagation rates, but parasite can still spread on both regions. In contrast, the subregions defined by the diffusion models here presented consist on a domain where infection spreads and another where it does not.

		Zero order kinetics				First order kinetics			
HLD (mm)	t_{90} (h)	ϕ_0	d_0	d_{RBC} (mm)	d_{IRBC}	ϕ_1	d_0	d_{RBC} (mm)	d_{IRBC}
0.06	18 s	0.04	NA	NA	NA	0.05	NA	NA	NA
0.09	45 s	0.06	NA	NA	NA	0.07	NA	NA	NA
0.2	4 min	0.13	NA	NA	NA	0.16	NA	NA	NA
0.4	10 min	0.23	NA	NA	NA	0.29	NA	NA	NA
0.6	1 h	0.41	NA	NA	0.5	0.5	NA	NA	NA
1.0	1.5	0.67	NA	NA	0.48	0.82	NA	NA	0.48
1.1	1.9	0.75	NA	NA	0.21	0.93	NA	NA	0.21
1.5	3.6	1.04	NA	NA	0.18	1.28	NA	NA	0.19
2.0	6.4	1.38	1.2	1.3	0.13	1.7	NA	NA	0.14
2.2	7.4	1.49	1.1	0.9	0.09	1.84	NA	NA	0.14
2.9	13.2	1.99	0.7	0.6	0.06	2.46	NA	NA	0.07

Table 3.8: *Charecteristic parameters of the reaction-diffusion balance in the haematocrit layer as a function of its depth (HLD). Characteristic diffusion times ($t_{90} \simeq 7\psi^2$). Thiele modulus (ϕ) and characteristic lengths for zero order and first order kinetics: depletion depth (d_0) with substrate concentration $C(d_0) = 0$; threshold depth for RBC viability (d_{RBC}) with $C(d_{RBC}) = 2.4\Delta 10^{-5} mols/l$; and threshold depth for IRBC viability (d_{IRBC}) with $C(d_{IRBC}) = 2.4\Delta 10^{-3} mols/l$. NA stands for non applicable, meaning that the threshold concentration values are not reached.*

3.5.2 Explicit model of the diffusion process

The individual-based approach deals with the reaction-diffusion problem stated in Equation 3.9 accounting for $U(C(\overrightarrow{x}, t)$ with the model of the individual cells and solving diffusion through the haematocrit layer with the model of the local environment.

The simplest numerical method to model diffusion through a discrete spatial grid is the explicit approach Forward-Time- Centred-Space (FTCS). Diffusion is solved iteratively at each time step by converting the spatial derivates at each point of the grid ($\overrightarrow{x}$) to finite differences, and the temporal derivates to finite increments to be transferred at the end of the time step ($t \rightarrow t + 1$).

This method is used by INDISIM (see Equations 2.5 and 3.4 in 2 and 3 dimensions, respectively), and has the general form

$$C_{\overrightarrow{x}}^{t+1} = C_{\overrightarrow{x}}^{t} + \widetilde{D} \sum_{i \in nn(\overrightarrow{x})} w_i C_i^t \tag{3.18}$$

where i is any of the spatial cells in the surroundings of $\overrightarrow{x}$, $nn(\overrightarrow{x})$, w_i is the weight of each contribution, and $\widetilde{D}$ is the numerical diffusion coefficient, which can be related

to the real experimental coefficient (D_{eff}) with a correction factor (cf) that depends on the discretization characteristic scales (spatial $l_{sc}$and temporal ts) of the model:

$$\widetilde{D} = cf \cdot D_{eff} = \frac{ts}{l_{sc}^2} \cdot D_{eff}$$

The numerical analysis of the method (Eq. 3.18) in one dimension reveals that the characteristic scales must fulfill $\widetilde{D} < \frac{1}{2}$ to maintain the numerical stability of the solution (Hoffmann and Chiang, 2004). This means that $ts < \frac{l_{sc}^2}{2 \cdot D_{eff}}$, otherwise numerical errors propagate and multiply through the spatial grid, completely altering the simulation outcome. For models in 2D and 3D, this constraint is $ts \leq \frac{l_{sc}^2}{D_{eff}} \cdot (1 - max\,(w)) < \frac{l_{sc}^2}{D_{eff}}$, where $max\,(w)$ is the maximum value of the diffusion weights as they appear in Equations 2.6 and 3.5 respectively.

When the size of the spatial cell is set to the scale of the RBC ($l_{sc} \sim 5\ \mu m$), the time step must fulfill $ts < \frac{l_{sc}^2}{D_{eff}} = \frac{10^{-7} cm^2}{10^{-6} cm^2/s} = 0.1\ s$. This time step is too small to simulate the long-term evolution of cultures (i.e. $48\ h \sim 10^7 ts$). Choosing this time step would also entail that some of the cellular processes that are now considered with simple time-averaged models (such as cellular metabolism and uptake) would require more elaborated time-depending descriptions.

Alternatively, the time step can be set to the current value ($ts = 6$ minutes, which is small enough to correctly account for merozoite propagation through the HL and big enough to use simple average models for the RBC metabolism), and the size of the spatial cell can be fixed to fulfill numerical stability. In this case $l_{sc} > \sqrt{\frac{ts}{1 - max\,(w)} \cdot D_{eff}} = 0.02\ cm$. Adopting this scale would entail that each spatial cell contains $\sim 10^4$ RBCs. Consequently, many of the current models (such as the release and spreading of merozoites) wouldn't be correctly implemented.

The FTCS approach forces a compromise regarding the characteristic scales of the model, between representing the spreading of the parasite (and a coarse model of the RBC) or the substrate diffusive limitations (and a detailed model of the RBC). The solution employed in INDISIM-RBC so far ($l_{sc} \sim 10\ \mu m$, $ts \sim 6$ minutes) opts for the former, and banks on the spreading of the parasite as the limiting factor to the propagation of the infection. The numerical diffusion coefficient corresponding to this choice ($\widetilde{D} = \frac{ts}{l_{sc}^2} \cdot D_{eff} \sim \frac{10^2 s}{10^{-6} cm^2} \cdot 10^{-6} cm^2/s \sim 10^2$) leads to the numerical instability of the diffusion model.

So, the values of $\widetilde{D}$ and the algorithm employed in the INDISIM-RBC simulations either overestimate the restrictions to diffusion whenever $\widetilde{D} < 1$, or do not consider diffusion limitations at all when $\widetilde{D} = 1$. The diffusion limitations observed in the simulations with

arbitrary values of $\widetilde{D}$ (for instance, $\widetilde{D} = 0.8$ in Figure 2.15b, in Section 2.3.5) correspond to excessively small values of the real D_{eff}.

Yet, the analysis of the reaction diffusion problem obtained in section 3.5.1 states that diffusion is indeed a limiting factor. FTCS simulations of diffusion alone carried out in an empty spatial grid using appropriate scales ($l_{sc} \sim 1\ \mu m$ and $ts \sim 1\ ms$, $\widetilde{D} \approx 0.3$) show that there are differences in the concentration of glucose in the scales employed by INDISIM-RBC (after 6 minutes, the relative difference in concentration observed at a RBC distance is $\delta = \frac{\triangle C(L=10\ \mu m; t=6\ minutes)}{\triangle C(L=10\ \mu m; 0)} \sim 10^{-3}$). This is the amount of nutrient that is not transported during a time step, so it can be assumed that $\widetilde{D} = 1 - \delta$.

This result is consistent with the application of values of $\widetilde{D} < 1$ above mentioned. The problem when trying to set the value for $\widetilde{D}$ in INDISIM-RBC is that the value calculated using smaller fractions of the spatial cell and time steps is not a scale invariant, in other words, that $\widetilde{D}$ varies with the resolution of the simulation. The discussion above indicates that diffusion plays a limiting role at the characteristic scales of the modeled system but our explicit models can not account for it satisfactorily.

3.5.3 Implicit model of the diffusion process

An alternative to the explicit resolution of any numerical problem is to use an implicit method. Implicit methods give the future configuration of the system by solving an equation that involves both the present and future states of the system.

The implicit Crank-Nicholson (C-N) method (Hoffmann and Chiang, 2004) can be employed to numerically solve diffusion within the haematocrit layer with a 1D model and the discretization used by INDISIM-RBC.

The reaction-diffusion process described by Equation 3.10 can be expressed with a finite difference approximation. Discretization of $\widetilde{C}(\zeta, \tau)$ leads to a grid containing N sites ($6 < N < 290$ to cover the range of observed HLDs using the scales $l_{sc} \sim 10\ \mu m$ and $ts \sim 6$ minutes), each one characterized by its instantaneous concentration $\widetilde{C}_i^\tau$. Equation 3.10 results in a linear system containing N coupled equations, one for each spatial cell i, to be solved at each time step (τ).

The explicit method described in the previous section (Equation 3.18) takes the form of Equation 3.19. For each equation i, the FTCS scheme assumes one unknown variable ($\widetilde{C}_i^{\tau+1}$) to be determined through a linear combination of known values at neighbour sites $\widetilde{C}_i^\tau$, $\widetilde{C}_{i+1}^\tau$ and $\widetilde{C}_{i-1}^\tau$.

$$\frac{\widetilde{C}_i^{\tau+1} - \widetilde{C}_i^\tau}{\triangle \tau} = \widetilde{D} \frac{\widetilde{C}_{i+1}^\tau - 2 \cdot \widetilde{C}_i^\tau + \widetilde{C}_{i-1}^\tau}{(\triangle \zeta)^2} - U_i^\tau \quad ; \quad i = 1 : N \tag{3.19}$$

Alternatively, Equation 3.10 can be represented by the set of N linear equations that constitute the implicit C-N approach. This results in the following system of equations, one for each site i:

$$\frac{\widetilde{C}_i^{\tau+1} - \widetilde{C}_i^{\tau}}{\triangle\tau} = \widetilde{D}\frac{\widetilde{C}_{i+1}^{\tau+1} - 2\cdot\widetilde{C}_i^{\tau+1} + \widetilde{C}_{i-1}^{\tau+1}}{(\triangle\zeta)^2} - U_i^{\tau} \quad ; \quad i = 1:N \tag{3.20}$$

In this case, each equation contains three unknown values ($\widetilde{C}_i^{\tau+1}$, $\widetilde{C}_{i-1}^{\tau+1}$ and $\widetilde{C}_{i+1}^{\tau+1}$) regarding the future concentration at the present and neighbour sites and only two known values ($\widetilde{C}_i^{\tau}$ and U_i) that include the information regarding the present state of site i. The C-N scheme can be expressed in the generalized form:

$$a_i\cdot\widetilde{C}_{i-1}^{\tau+1} + b_i\cdot\widetilde{C}_i^{\tau+1} + c_i\cdot\widetilde{C}_{i+1}^{\tau+1} = D_i^{\tau}$$

where D_i^{τ} is a linear combination of $\widetilde{C}_i^{\tau}$ and U_i. This set of equations, together with boundary conditions (i) $\widetilde{C}_N^{\tau} = 1$, and (ii) $\frac{\partial\widetilde{C}_0^{\tau}}{\partial t} = 0$, stated in Section 3.5.1, can be expressed in the matrix form:

$$\begin{pmatrix} b_2 & c_2 & & & \\ a_3 & b_3 & c_3 & & \\ & & \ddots & & \\ & & a_{N-3} & b_{N-2} & c_{N-1} \\ & & & a_{N-2} & b_{N-1} \end{pmatrix} \begin{pmatrix} C_2^{\tau+1} \\ C_3^{\tau+1} \\ \vdots \\ C_2^{\tau+1} \end{pmatrix} = \begin{pmatrix} D_2^{\tau} \\ D_3^{\tau} \\ \vdots \\ D_2^{\tau} \end{pmatrix} \quad \Rightarrow \quad C^{\tau+1}\cdot A = D^{\tau} \tag{3.21}$$

Matrix A in Equation 3.21 is determined and tridiagonal. It can be inverted to determine $C_i^{\tau+1}$, $\forall i$. The results obtained with such an approach are consistent with the analytical results presented in Section 3.5.1.

This implicit formulation of the reaction-diffusion problem can be worked out through different numerical methods. The main advantage of such type of algorithms is that they are numerically stable regardless the size of the spatial and temporal scales. These methods can also be implemented in INDISIM-RBC in order to solve the diffusion of substances. Their most important drawbacks are i) that the inversion and solution of matrix A requires a lot of computational effort, and ii) that the differences in the individual uptake (and the consequent heterogeneities in substrate concentration appearing in the haematocrit layer) can lead to ill conditioned matrixes, not amenable to to computational solving.

Implementing C-N in INDISIM-RBC would entail extending the presented formulation

to two and three dimensions. The extension of this reaction-diffusion problem to 2D and 3D entails dealing with band diagonal matrixes, analogous to the one appearing in Equation 3.21, but with each line i containing nn number of terms per row (representing the total number of spatial cells that constitute the nearest neighbourhood of cell i). Matrix A in 2D contains $nn = 5$ terms per row when only side neighbours are taken into account, and $nn = 9$ when diagonal nearest neighbours are also included. Matrix A in 3D can contain up to $nn = 27$ terms when all the first neighbour cells are considered. The number of operations to be carried out at each time step linearly increases with N and the computational time also increases with the number nn.

The study of the optimal computational methods used to solve partial differential equations under different constraints (such as the present reaction-diffusion problem in the HL) constitutes a research field in computational physics on its own. Built-in libraries and numerical packages prepared to solve diffusion using optimized implicit methods are available from several academic sources but none could be properly assembled to INDISIM-RBC. At the present moment, the implicit solution of the diffusive model remains an unresolved problem to be tackled in further works.

3.6 Discussion and open questions

INDISIM-RBC.*v3D* improves the set of rules governing individuals (RBCs and IRBCs) and the rules describing the environment (spatial structure, extracellular parasite and substrate concentration) to better account for local interactions and transport phenomena (Section 3.2). Three representational goals have been achieved with the 3D version of the model (Section 3.3):

1. *Population dynamics and structure:* The temporal evolution of parasitaemia ($\%I$), infection growth ratio (GR) and distribution of post-invasion times among IRBCs ($q\left(t_{INF}\right)$) observed in short-term and long-term culture systems are still quantitatively reproduced by the model.

2. *Spatial structure of the hematocrit layer:* the RBC packing factor within the hematocrit layer (pf) in the model is consistent with the cell density measured for the settled hematocrit in experimental systems.

3. *Infection dynamics:* the distribution of IRBCs with (k) multiple invasions predicted by the model ($f(k; P_{inf})$) is in accordance with the experimental observations ($f_{obs}(k)$).

Yet, the foremost advantage of this version is that it allows tackling static *in vitro* culture systems with different macroscopic geometries and comparing them one with each other (Section 3.4). The study of different experimental setups shows that optimal harvests are obtained with the following ranges: depth of the hematocrit layer $0.2\ mm < HLD < 0.5\ mm$ and distances between walls of the culturing vial $L > 2\ cm$.

INDISIM-RBC.*v3D* alone does not provide a justification for these ranges. However, when additional top-down phenomenological laws are assumed, the behaviour of real systems is accurately reproduced. These whole-system laws basically consist in splitting the hematocrit layer into different subregions with high/low infection proliferation rates. They lead to the decrease in GR for high values of the hematocrit layer depth (when $HLD > 0.48\ mm$) and define a minimum threshold for the separation between walls. The reduction in GR observed for smaller cultures ($HLD \sim 0.1\ mm$) can be explained through individual-based limitations resulting from the discrete nature of individual interactions.

A continuous model for diffusion of substrate and waste products has been developed to provide an explanation of the phenomenological laws, although it has not yet been assembled to the individual-based approach (Section 3.5).

Further work in the study of geometric limitations on the static cultivation of the parasite should address the implementation of a model for diffusion that can give rise to the limitations in real culture systems. Nevertheless, it must be kept in mind that the restrictions observed in experiments may be caused by other factors, besides diffusion limitations. For instance, they might be caused by unaccounted influences of the spatial structure of the hematocrit layer, merozoite spreading or RBC invasion. Anyhow, the analysis of static *in vitro* systems still offers questions to unravel.

Changing to another topic, INDISIM-RBC can also be modified to account for cultures in suspension. In this case, the model of the invasion of healthy RBCs should be revisited. The development of a model that can correctly describe both static and agitated culture systems would be of great interest in order to design and build an operative and reliable bioreactor-like culturing device.

Apart from the application-oriented contributions of this model, the process of building INDISIM-RBC has provided interesting results in the ambit of individual-based modeling of microbial communities. In Chapter 4, some of these general conclusions are exposed and the results obtained with INDISIM-RBC are considered in a broader mark, together with similar results obtained with other versions of INDISIM and with other approaches.